A Cell Method Stress Analysis in Thin Floor Tiles Subjected to Temperature Variation

E. Ferretti[1]

Abstract The Cell Method is applied in order to model the debonding mechanism in ceramic floor tiles subjected to positive thermal variation. The causes of thermal debonding, very usual in radiant heat floors, have not been fully clarified at the moment. There exist only a few simplified analytical approaches that assimilate this problem to an eccentric tile compression, but these approaches introduce axial forces that, in reality, do not exist. In our work we have abandoned the simplified closed form solution in favor of a numerical solution, which models the interaction between tiles and sub-base more realistically, when the positive thermal variation increases the volume of the sub-base. The thermal problem has been approached as a contact problem in a composite structure. In particular, the kinematic and equilibrium conditions have been imposed at the interface between lower part, which is the sub-base, and the upper part, which is composed by the adhesive, the tiles, and the grouting between the tiles. The failure condition has been studied in the Mohr-Coulomb plane by using the Leon criterion, a unifying criterion that combines the shear stress with traction and compression. Therefore, we employed a unique failure criterion both for the nodes at the interface between sub-base and adhesive (which undergo a shear/tensile failure or a shear failure) and the nodes at the interface between tiles and grouting (which undergo a tensile failure). This allowed us to model the tile debonding both in the horizontal and in the vertical interfaces, while previous FEM codes treated the tile debonding only on the horizontal interfaces. The numerical analyses were performed in parametric modality, by varying the geometric and mechanical characteristics of the model. Particular attention was devoted to the modeling of thin tiles, a new type of ceramic tiles, for which there are no yet consensus standards.

Keywords: Thin Tiles, Composite Structures, Contact Problem, Failure criteria, Cell Method, Parametric Analysis

[1] DICAM – Department of Civil, Environmental and Materials Engineering, Scuola di Ingegneria e Architettura, Alma Mater Studiorum, Università di Bologna, Viale Risorgimento 2, 40136 (BO), ITALY.

1 Introduction

One of the hottest trends in floor tile market is the emergence of thin tiles. There are three categories of products being marketed as thin tiles. In the first category, tiles are formed using the traditional dust pressing methodology. In the second and third category, tiles are formed using a lamina process, reinforced with fiberglass or polymeric backing materials in the last case. Regardless of category, thin tiles have a much lower breaking strength than regular ceramic tiles. They also are less able to resist impact loading when unsupported.

The main reason for looking at the performance of thin tiles in particular is because of the increasing availability of thin tiles in the floor tile market. This, in turn, is a consequence of a whole range of advantages for manufacturers coming from tiles engineered to be thinner, including carrying out installations over existing floors, eliminating the need for ripping out existing finishing materials in renovation projects, and saving time and money in labor costs.

Made of porcelain, the thin tiles start at thicknesses of about 2.5 *mm* for walls, going up to about 6 *mm* for floors, while, until recently, floor tiles were 8 to 12 *mm* thick. Thin tiles are lightweight, reduce material consumption and require the use of fewer resources to manufacture and ship them.

The question we are trying to answer in this paper is whether or not thin tiles behave better than traditional floor tiles when used on radiant heat floors (Fig.1). In particular, we want to investigate whether using thin tiles would avoid the principal problem of heat radiant floors made from traditional tiles, that of tile separation from the sub-base when the temperature increases (Fig.2).

We treated the radiant heat floor as a composite structure, made up of a lower part, the sub-base, and an upper part, composed of the adhesive, the tiles and the grouting between the tiles (Fig.3). The analysis was performed on the vertical cross section, by using the Cell Method (the CM [Tonti (2001); Ferretti (in press)]), and the failure condition was evaluated both for the adhesive, as in Dong and Atluri (2012), and for the vertical interfaces (between tiles and grouting).

The lower part is the one where the variation in temperature takes place, causing the lower part to change in volume (Fig.4). If the lower part were not bound to the upper part, the change in volume would occur without generating stresses inside the lower part (Fig.4). Actually, the lower part is free to move horizontally over the laying surface, due to the presence of expansion joints at each end of the run of tiles and a thermal insulation layer on the laying surface (Fig.1). This means that the lower part is constrained isostatically and, consequently, the thermal gradient does not induce any stress in it.

When the lower part is bound to the upper part (Fig.5), its constraint degree be-

1) **Slab in brick and cement**
2) **Perimeter joint**
3) **Tiles**
4) **Screed**
5) **Insulating panel and water pipes**
6) **Vapor barrier**
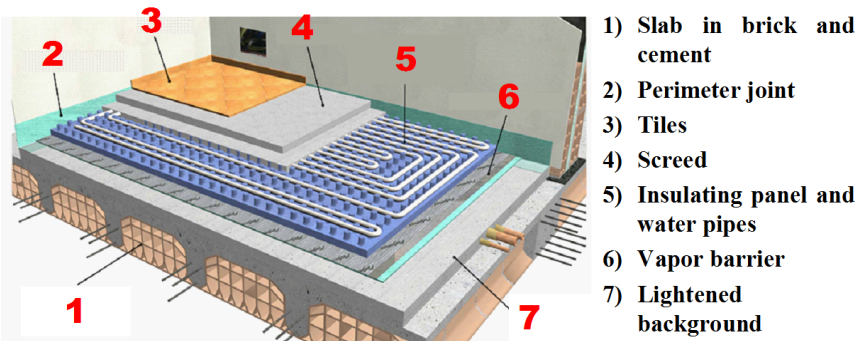7) **Lightened background**

Figure 1: Components of a radiant heat floor

Figure 2: Tile separation from the sub-base in a radiant heat floor [Cocchetti, Comi, and Perego (2011)]
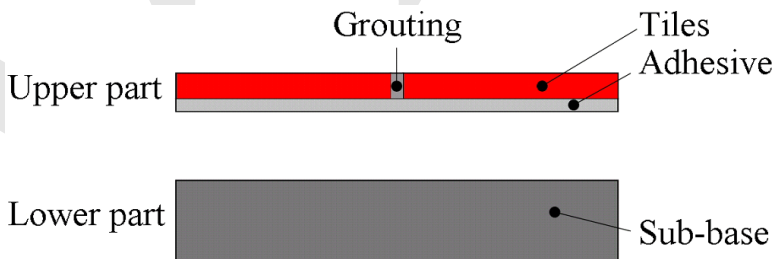

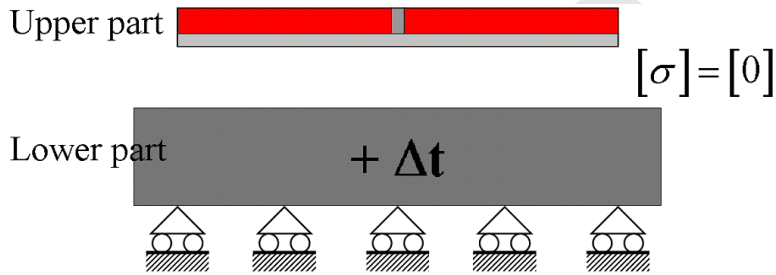Figure 3: Components of the upper and lower parts in the numerical model

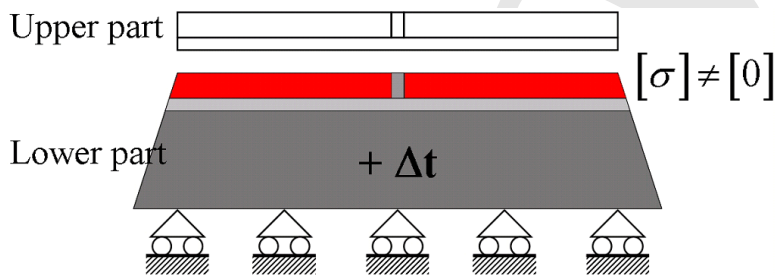Figure 4: Variation in temperature in the sub-base: isostatic sub-base

Figure 5: Variation in temperature in the sub-base: hyperstatic sub-base

⁶⁹ comes hyperstatic and the interaction between the two parts generates stresses in
⁷⁰ both of them. In the present paper, the interaction between upper and lower parts
⁷¹ has been approached as a contact problem, a boundary condition that is easy to treat
⁷² with the CM, as shown in Ferretti (2013), Ferretti (2004b), and Ferretti (2003a,b),
⁷³ while it is not at all trivial in the differential formulation [Boe, Rodriguez, Plazaola,
⁷⁴ Banfield, Fong, Caballero, and Vega (2013); Imai and Nakagawa (2012); Blázquez
⁷⁵ and París (2011); Chen, Cui, Nie, and Li (2011); Yun, Junzhi, Yufeng, and Yiqiang
⁷⁶ (2011); Hartmann, Weyler, Oliver, Cante, and Hernández (2010); Selvadurai and
⁷⁷ Atluri (2010); Theilig (2010); Zhou, Li, Yu, and Lee (2010); Chen and Atkinson
⁷⁸ (2009); Reaz Ahmed and Deb Nath (2009); Willner (2009); Han, Liu, Rajendran,
⁷⁹ and Atluri (2006)].

⁸⁰ The amount of interaction depends on the geometric parameters of the model,
⁸¹ specifically the thickness of the adhesive, the thickness of the tiles, the length of
⁸² the tiles, the number of tiles and the thickness of the grouting. It also depends
⁸³ on the mechanical parameters of the adhesive, the Young modulus and the Poisson
⁸⁴ modulus. We wish to investigate the effect that each of these parameters have on the
⁸⁵ separation process. To achieve this, we performed numerical analysis in parametric
⁸⁶ modality, allowing the operator to define all the parameters.

2 Some features of the CM code for crack propagation analysis

Our choice of the CM for the analysis is based on its high degree of detail, which allows us to clarify the mechanisms of stress transfer between the components of the floor. In particular, the CM is capable of capturing corner effects [Ferretti, Casadio, and Di Leo (2008)], providing us with an insight into how stress concentration at the corners of the tiles modifies the principal directions of stress, causing twisting at the corners (Fig. 6). Some examples of how the corner effects are treated in the differential formulation can be found in Zhang (2011), Zheng and Li (2012) and Schnack, Weber, and Zhu (2011).

The picture of the principal directions of stress in Fig.6 was plotted for an increase in temperature in the sub-base, with the length of each segment being proportional to the intensity of the stress at that point. The main principal stresses are those along the horizontal direction, with the sub-base being compressed (blu lines), while the adhesive, the grouting and the tiles are tensioned (red lines). The horizontal compression in the sub-base occurs because the upper part, to which it is bonded, restricts it from expanding freely along the horizontal direction, counteracting the increase in volume of the sub-base that takes place when the temperature increases (Fig.5).

Moreover, we can also see that there is interaction between the tiles and the grouting along the vertical interfaces (Fig.7): the condition of perfect adherence, together with the difference between the two elastic modules, leads to the tiles stretching the grouting along the vertical direction, while the grouting compresses the tiles along the vertical direction. As a consequence, both principal stresses in the grouting are tensile stresses, while the vertical principal stress in the tiles is a compression stress. This phenomenon is clearer in Fig.8, with the colors indicating the sign and the intensity of the vertical normal stresses. Once again, the vertical stress in the tiles is compression stress, while the vertical stress in the grouting is tensile stress.

The deformed configuration in Fig.8 was plotted by amplifying the displacements 100 times. This also makes evident the Poisson effect on the grouting.

The analysis was performed under plane strain conditions and the failure condition was evaluated in the Mohr/Coulomb plane. As is well known, the Mohr criterion (Fig.9) has a bi-linear failure surface, which fits the failure condition in compression well, but it underestimates the ultimate strength for pure shear stress and is unable to calculate the correct direction of propagation both for uniaxial tensile load and pure shear. Since crack propagation in floors takes place, prevalently, due to a combination of traction and shear, the Mohr criterion should be replaced with a criterion that is more restrictive along the axis of uniaxial tensile load. The criterion used here is the Leon criterion [Ferretti (2004a,b); Ferretti (2009)], whose limit sur-
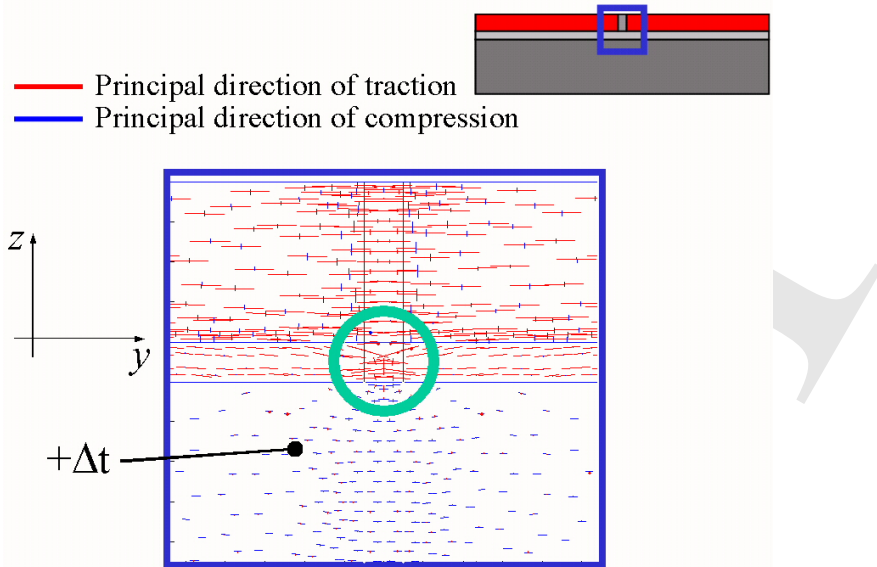
Figure 6: Twisting of the principal directions of stress at the corners of the tiles
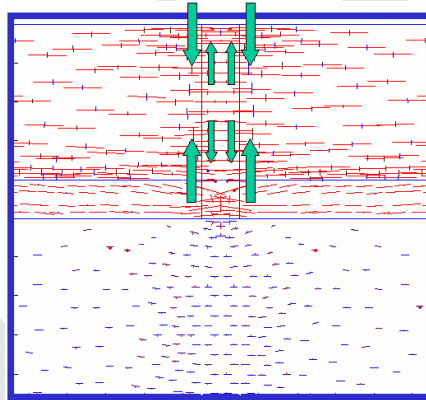

Figure 7: Interaction between the tiles and the grouting, along the vertical interfaces

125 face has a parabolic shape (Fig.10). The tensile strength for Leon, σ_L, lower than
126 that for Mohr, σ_M, is exactly equal to the tensile strength in uniaxial tensile load,
127 σ_t.

128 The analysis in the Mohr/Coulomb plane was performed for the twin nodes of the
129 vertical interfaces between tiles and grouting and for the twin nodes of the laying
130 surface. Each pair of twin nodes provides one point in the Mohr/Coulomb plane,
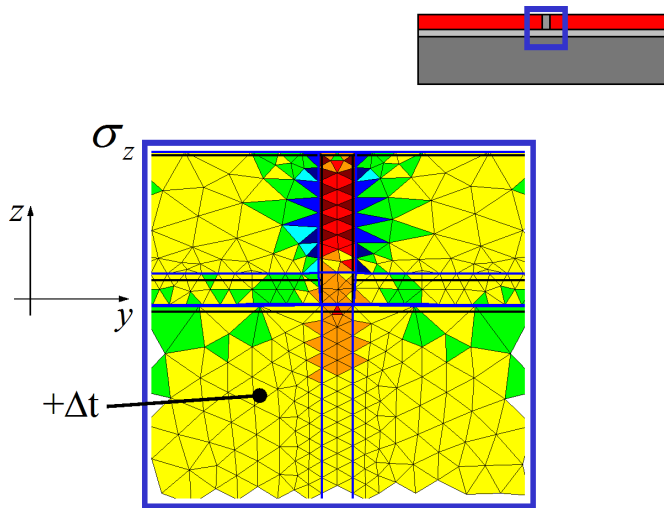
Figure 8: Vertical normal stresses for an increase in temperature in the sub-base
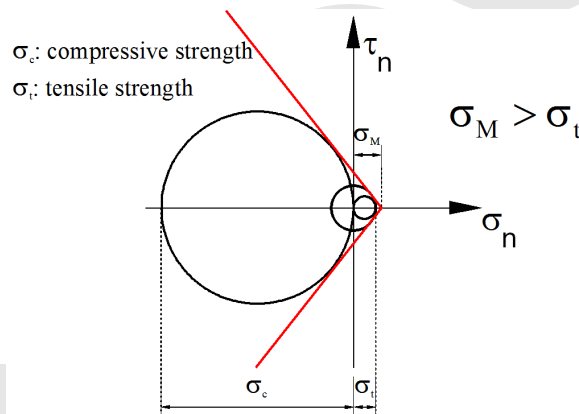
Figure 9: Failure criterion of Mohr and greater circles of Mohr for uniaxial traction, uniaxial compression and pure shear

whose coordinates are the normal and shear stresses in the twin nodes, evaluated over the interface plane.

For this particular application, the direction of propagation is known, because the crack propagates along the interface. Thus, in order to identify the direction of propagation, we do not need to build the three circles of Mohr, which give the state of stress at the point, for all the planes passing through the point. Moreover, since the point drawn for the interface plane at the limit condition is the failure point
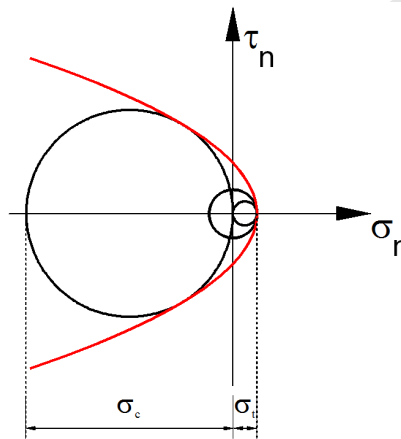
Figure 10: Failure criterion of Leon and greater circles of Mohr for uniaxial traction, uniaxial compression and pure shear
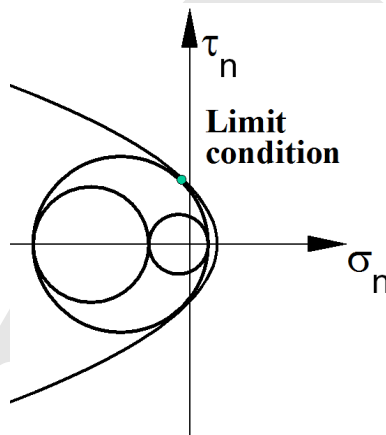
Figure 11: Failure point and circles of Mohr for the twin nodes which are releasing

138 (Fig.11), we know that, under the assumption of having plotted the circles of Mohr
139 for the limit condition, the greater circle would be tangent to the limit surface of
140 Leon just in the point drawn for the interface plane (Fig.11). With this in mind,
141 evaluating the factor of safety with respect to the propagation is very simple: it is
142 given by d, the distance between the point drawn for the interface plane and the
143 limit surface of Leon (Fig.12), with d greater than zero in safety (Fig.12) and equal
144 to zero when the crack starts propagating (Fig.11).
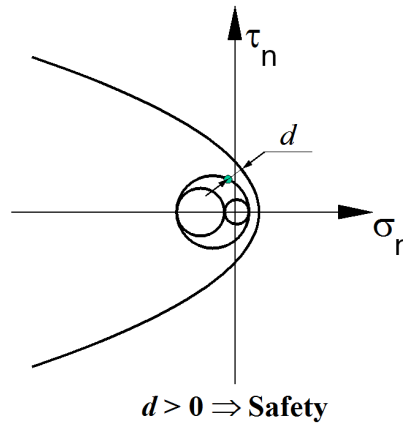
$$d > 0 \Rightarrow \textbf{Safety}$$

Figure 12: Evaluation of the safety factor in the Mohr/Coulomb plane

3 Numerical results

Numerical analysis has been performed varying the number of tiles, the elastic modulus of the adhesive, the height of the tiles, the height of the adhesive and the thickness of the grouting.

The first model we considered is a simplified model made of just two thin tiles, each with a thickness of 4 *mm* (Fig.13). Both the adhesive and the grouting are 1 *mm* thick and the elastic modulus of the adhesive is $8000N/mm^2$.

The stress analysis was performed for an increase in temperature of $30°C$ from the reference temperature, which is the temperature at which the floor was constructed.

Since the first crack enucleates on the vertical interfaces, the ones between tiles and grouting, we have focused on the twin points of the vertical interfaces, plotting both the stress analysis in the plane of Mohr/Coulomb and the function of the safety factor (Fig.14), which is the same for both vertical interfaces. In Fig.14, we have also plotted the normal and shear stresses on the laying surface, between the adhesive and the sub-base.

For the initial variation in temperature, equal to $1°C$, all the points in the Mohr/Coulomb plane lie inside the failure surface and the factor of safety is greater than zero everywhere along the vertical interfaces (Fig.14). This means that this temperature does not induce any cracks along the vertical interfaces and the variation in temperature can be increased.

We can state the same for a variation in temperature of $2°C$ (Fig.15): all the points of the Mohr/Coulomb plane lie inside the limit surface and, consequently, the fac-
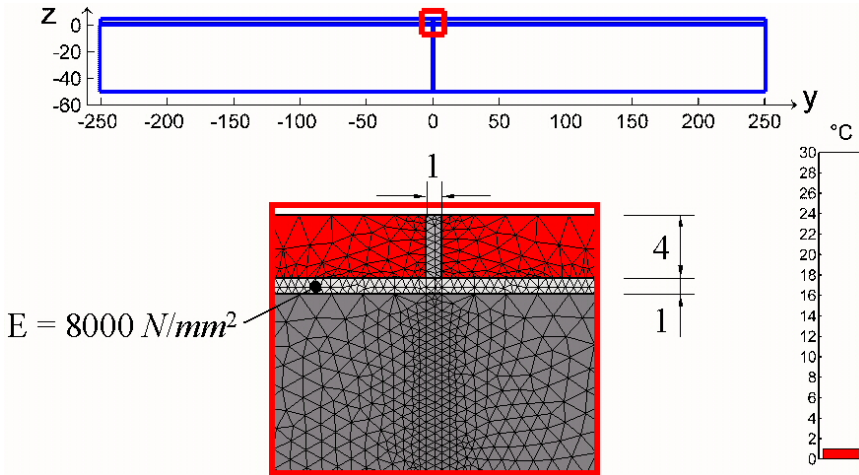
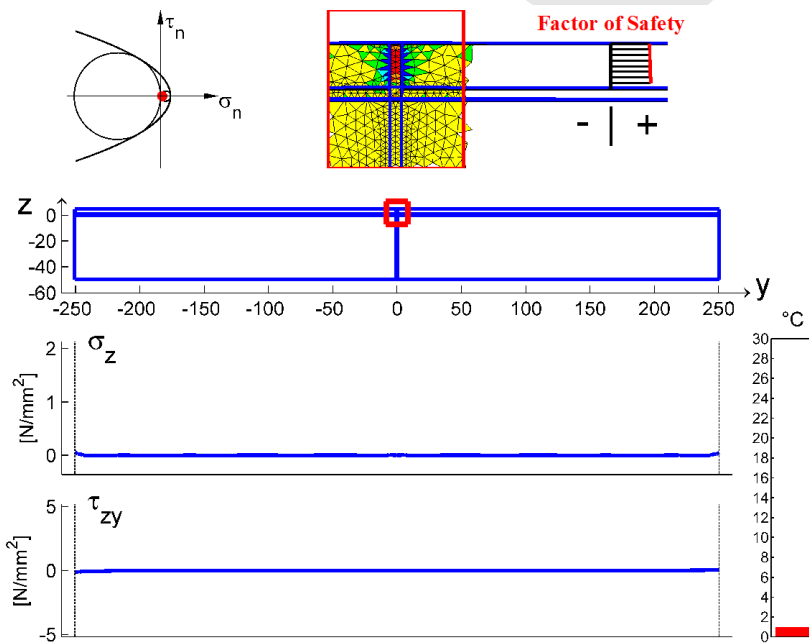Figure 13: Simplified model, made of two tiles

Figure 14: Stress analysis for an increase in temperature of $1°C$

167 tor of safety is greater than zero. Nevertheless, the points of the Mohr/Coulomb
168 plane are nearer to the limit surface, resulting in the factor of safety to decrease
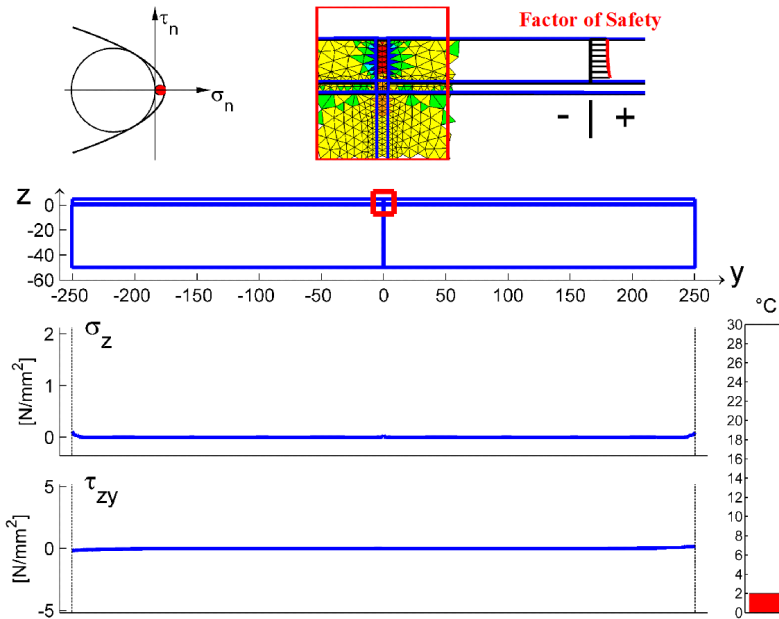
Figure 15: Stress analysis for an increase in temperature of $2°C$

169 everywhere along the vertical interfaces.

170 At the subsequent increase in temperature $(3°C)$, two points of the Mohr/Coulomb
171 plane reach the limit surface, just at the vertex of the parabola (Fig.16). This indi-
172 cates that a tensile failure condition has been reached on the vertical interfaces.

173 From the plot of the safety factor in Fig.16, we can see that the first points for which
174 the factor of safety is no longer greater than zero are those on the upper corners.
175 Thus, two cracks enucleate on the two upper corners and propagate downwards.

176 The failure of the vertical surfaces enhances the normal stress on the middle point of
177 the horizontal interface under the grouting (Fig.16). This kind of crack propagation
178 is brittle, in the sense that, each time a pair of twin nodes separates, the remaining
179 twin nodes turn out to be more stressed than previously and fail, progressively,
180 for the same value of temperature at which the cracks were enucleated (see Fig.17
181 for an intermediate step of crack propagation), leading the vertical interfaces to
182 separate completely and the stresses under the grouting to increase further (Fig.18).

183 At the end of the propagation process along the vertical interfaces, the principal di-
184 rections of stress and the principal stresses turn out to be highly modified (Fig.19).
185 The new distribution of the stresses can be easily explained in the light of hydrody-
186 namic analogy, taking into account that the two vertical cracks are two obstacles to
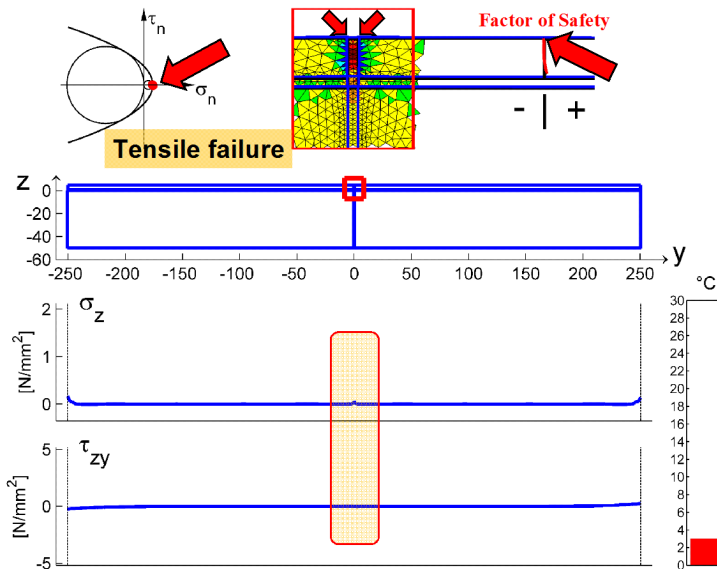
Figure 16: Stress analysis for an increase in temperature of $3°C$: first failure condition

the stress flow in the horizontal direction. This is the main cause of the arc effect, well visible in the sub-base.

The greatest difference between the stresses before and after the failure of the vertical interfaces can indeed be observed precisely in the sub-base, where the compression stresses along the horizontal direction have been replaced by tensile stresses arranged in a circle. The presence of traction in this position can explain the radial damage in the sub-base that often appears under the corners together with the separation of the tiles.

By letting the temperature increase further, the next failure condition is reached on the horizontal interface when the factor of safety becomes equal to zero or negative. This takes place at a variation of $7°C$ (Fig.20), with a tensile failure at the interface between the grouting and the sub-base. The consequence on the state of stress on the horizontal interface is a knocking down of the peak of the normal stress under the grouting (Fig.21).

This crack propagates at $11°C$ for tensile failure (Fig.22) and at $17°C$ for a combination of tensile and shear failure (Fig.23).

At $18°C$, we have the failure of the end nodes on the horizontal interface (Fig.24), with a knocking down at the ends both for the normal stress and the shear stress
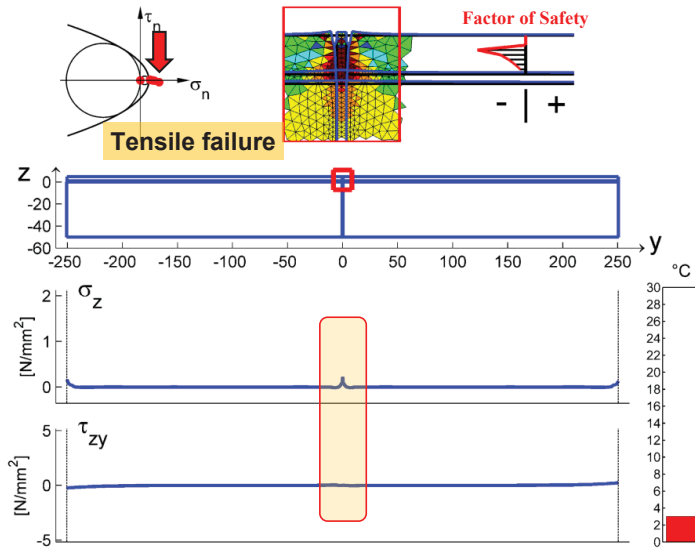
Figure 17: Stress analysis for an increase in temperature of $3°C$: intermediate step of crack propagation
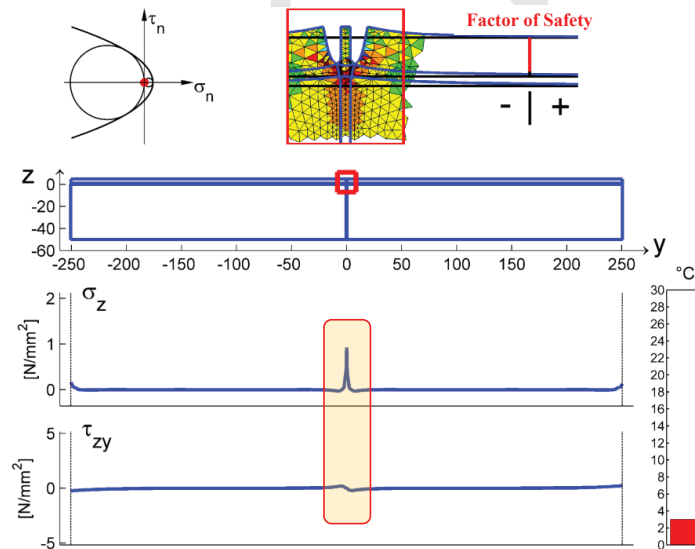

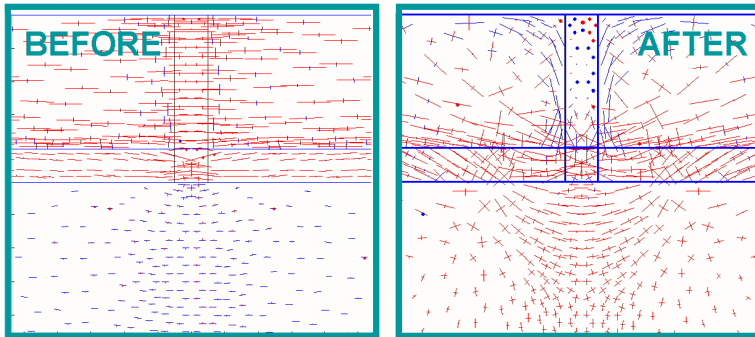Figure 18: Stress analysis for an increase in temperature of $3°C$: end of propagation

Figure 19: Principal directions of propagation before and after the failure of the vertical interfaces

(Fig.25). The crack under the grouting then extends at $19°C$ and $22°C$, for a combination of tensile and shear failures in both cases. Finally, at $24°C$, the crack on the horizontal interface extends into brittle failure (Fig.26), leading the two tiles to separate from the sub-base almost completely (Fig.28). Consequently, a variation in temperature of $24°C$ can be considered as the critical variation in temperature for this simplified model.

During all the propagation process on the horizontal interface, the kind of failure is a shear failure (Fig.27), because the points of the Mohr/Coulomb plane which mostly extrude from the limit surface are those on the shear axis.

At the end of the propagation process, temperature can be increased further, with the separation of a few other pairs of twin nodes on the horizontal interface. The final configuration is shown in Fig.29.

When increasing the number of tiles from 2 to 6, the numerical analysis provides similar results, in the sense that the crack will enucleate on the vertical interfaces also in this case, then under the grouting and, finally, on the ends of the horizontal interface. For each of the five groutings, the vertical cracks propagate downwards along the first of the two interfaces which fail (Fig.30) and upwards, from the adhesive to the upper corner, along the second interface (Fig.31).

The most interesting result is the one concerning the critical variation in temperature, which is $24°C$ even when there are 6 tiles (Fig.32).

The analyses performed for 3 and 4 tiles confirmed that the simplified model of just two tiles is able to capture the critical temperature even for models with a greater number of tiles (Fig.32).
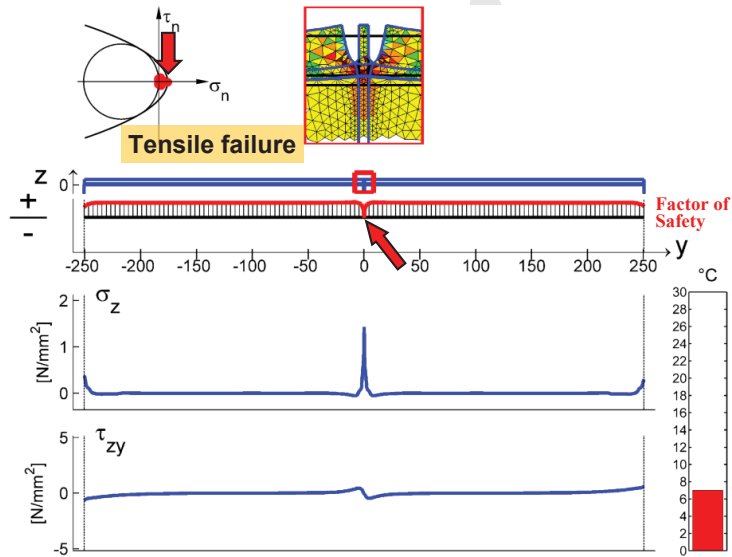
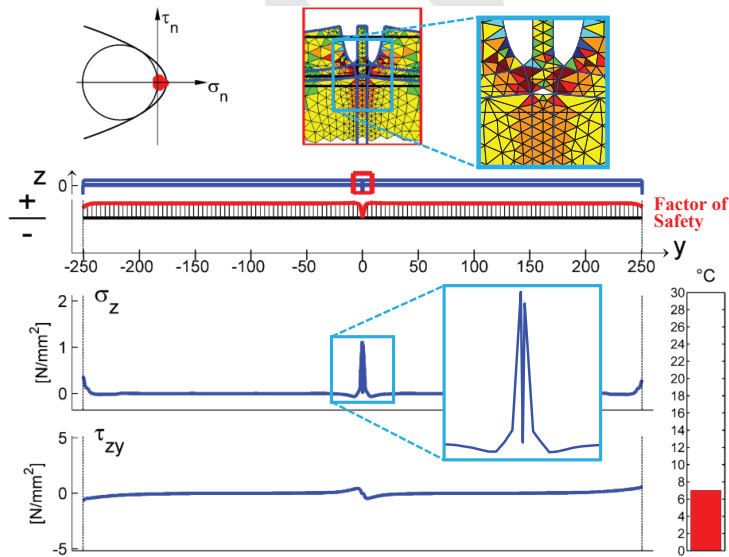Figure 20: Stress analysis for an increase in temperature of $7°C$: failure condition

Figure 21: Stress analysis for an increase in temperature of $7°C$: domain updating and knocking down of the stress peak
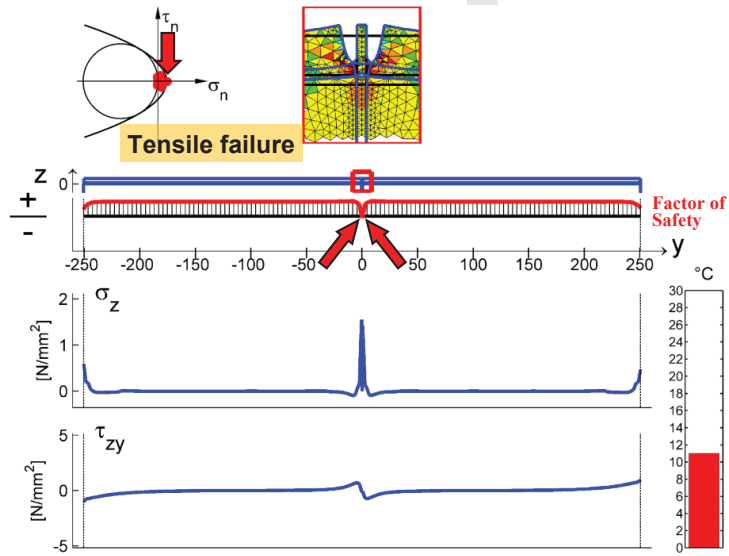
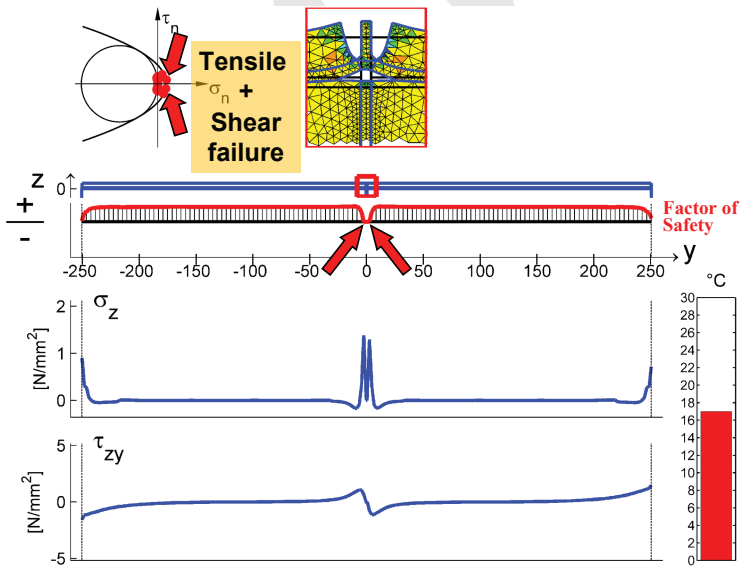Figure 22: Stress analysis for an increase in temperature of $11°C$

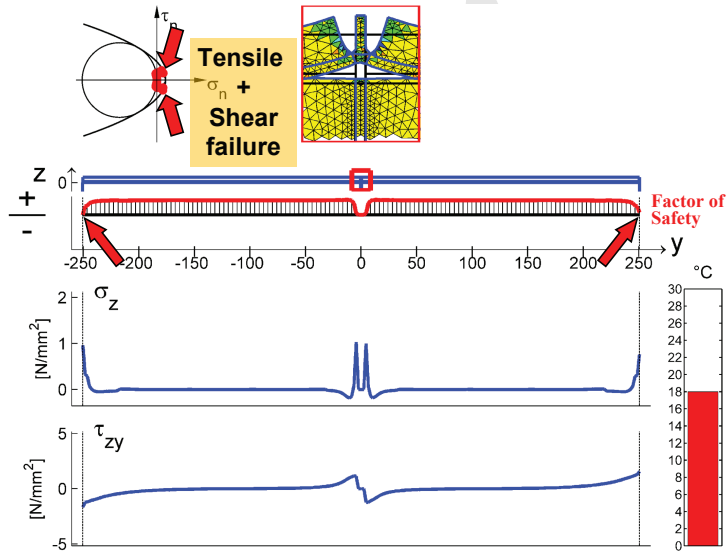Figure 23: Stress analysis for an increase in temperature of $17°C$

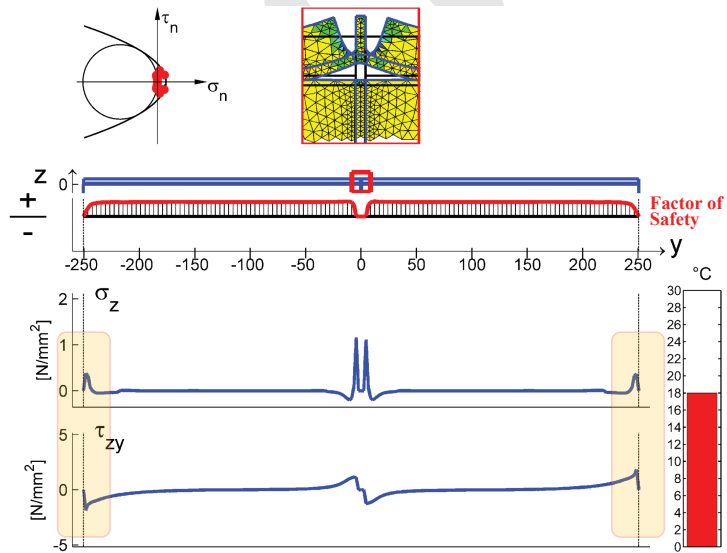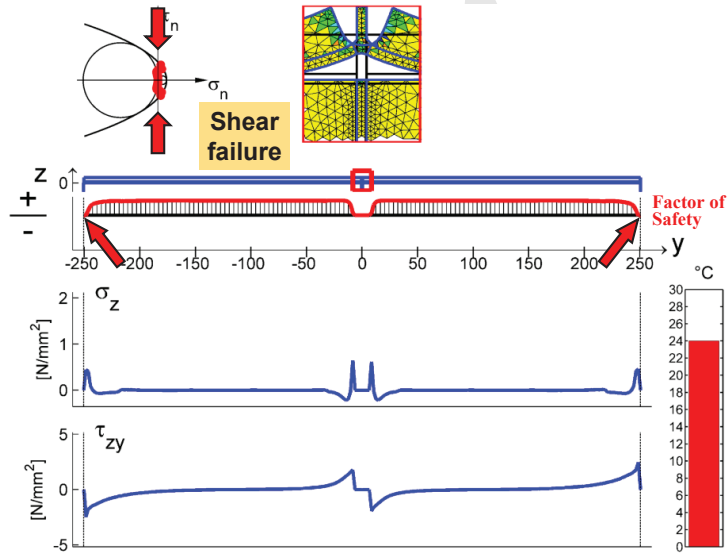Figure 24: Stress analysis for an increase in temperature of $18°C$: failure condition

Figure 25: Stress analysis for an increase in temperature of $18°C$: domain updating and knocking down of the stress peaks

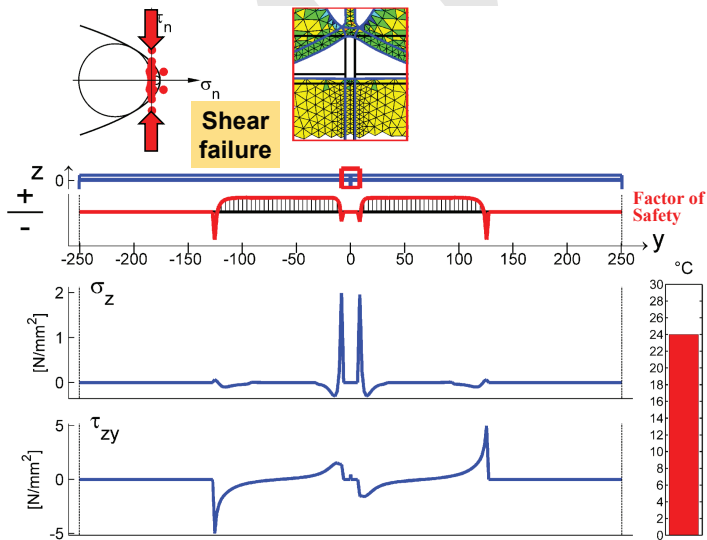Figure 26: Stress analysis for an increase in temperature of $24°C$: first failure condition

Figure 27: Stress analysis for an increase in temperature of $24°C$: intermediate step of crack propagation
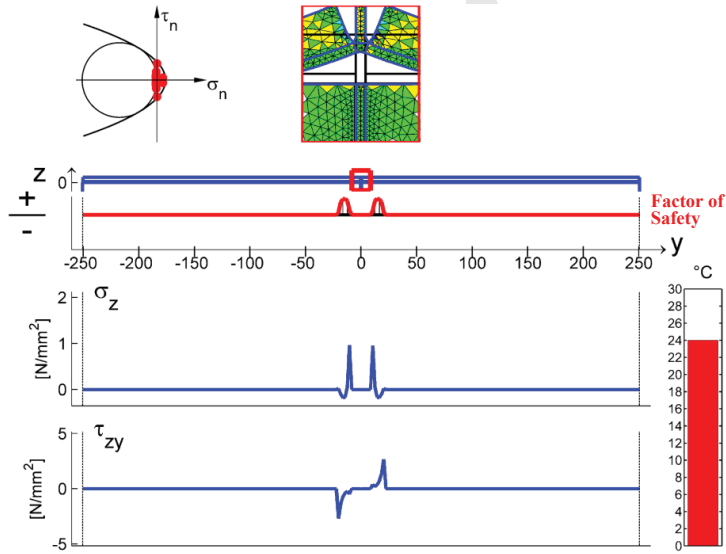
Figure 28: Stress analysis for an increase in temperature of $24°C$: final stage of crack propagation
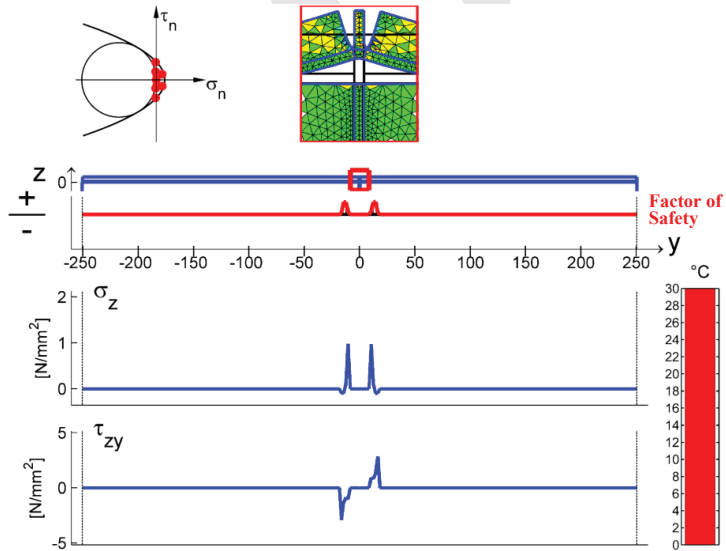

Figure 29: Stress analysis for an increase in temperature of $30°C$
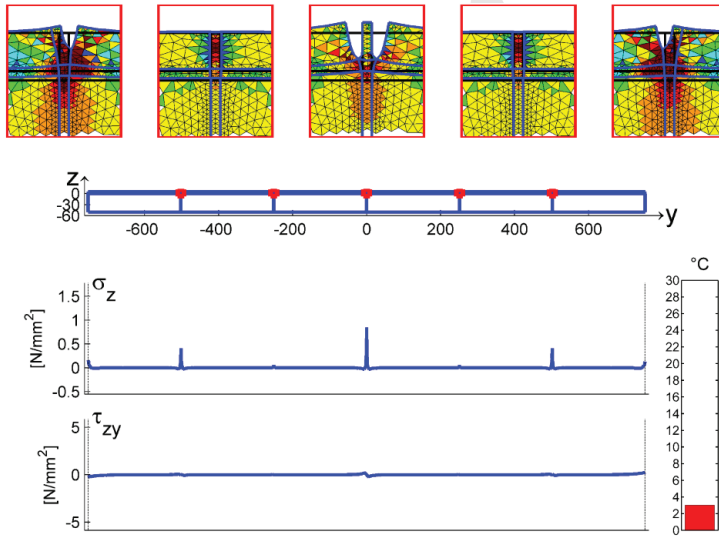
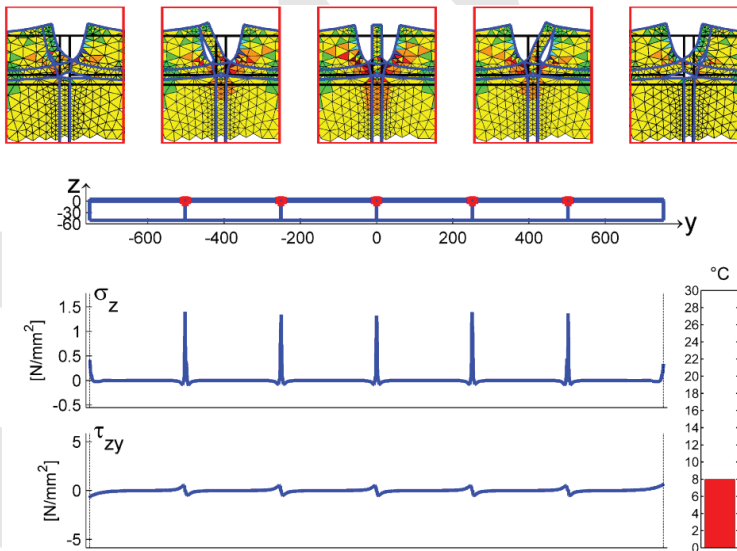Figure 30: Stress analysis on the model with 6 tiles: downward propagation along the first interface which fails

Figure 31: Stress analysis on the model with 6 tiles: upward propagation along the second interface which fails
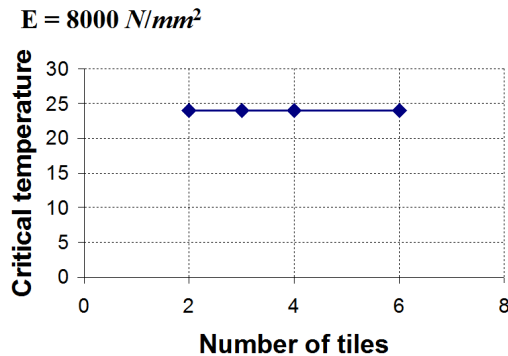
E = 8000 *N/mm²*

Figure 32: Critical temperature in function of the number of tiles for $E = 8000N/mm^2$

3.1 Parametric analysis on the elastic modulus of the adhesive and the number of tiles

Decreasing the stiffness of the adhesive from 8000 to $3500N/mm^2$ in the simplified model made of 2 tiles, we can notice two different effects on the crack propagation process. The first is the point of enucleation on the vertical interfaces, which is no longer at the upper corners, but at mid-height along the vertical interfaces (Fig.33). The vertical cracks at first propagate upwards and then downwards.

The second effect is the critical temperature, which increases from 24 to $29°C$ (Fig.34), with a gain of $5°C$ (Fig.35).

Similarly for the stiffer adhesive, in the model composed of 6 tiles, for each of the five groutings the vertical cracks propagate downwards along the first interface which fails, and upwards, from the adhesive to the upper corner, along the second interface. Moreover, also in this case, increasing the number of tiles does not change the critical temperature, which remains at $29°C$ (Fig.36). Since we can state the same for 3 and 4 tiles (Fig.37), we may therefore assume that the simplified models can predict the critical temperature even for the models with a greater number of tiles.

From the analyses on the elastic modulus of the adhesive, we can conclude that less stiff adhesives are preferable to stiffer adhesives, since they increase the critical temperature.
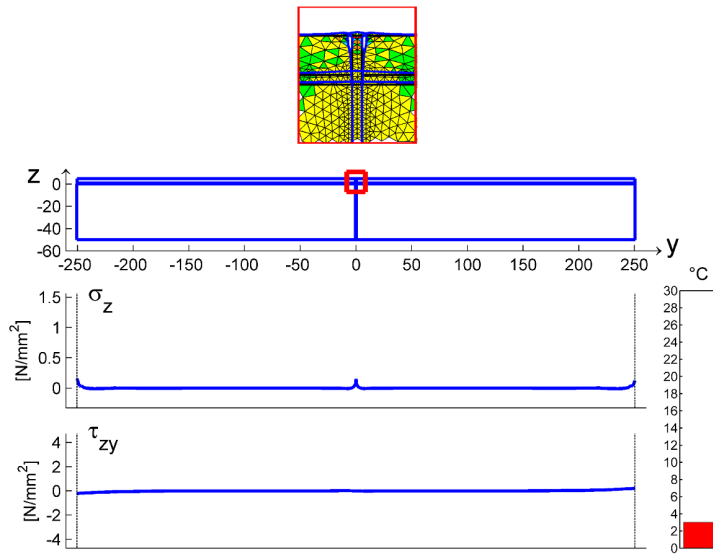
Figure 33: Crack enucleation along the vertical interfaces in the model made of 2 tiles

Figure 34: Stress analysis for the critical temperature in the model made of 2 tiles: final stage of crack propagation along the horizontal interface

Figure 35: Critical temperature in function of the elastic modulus of the adhesive
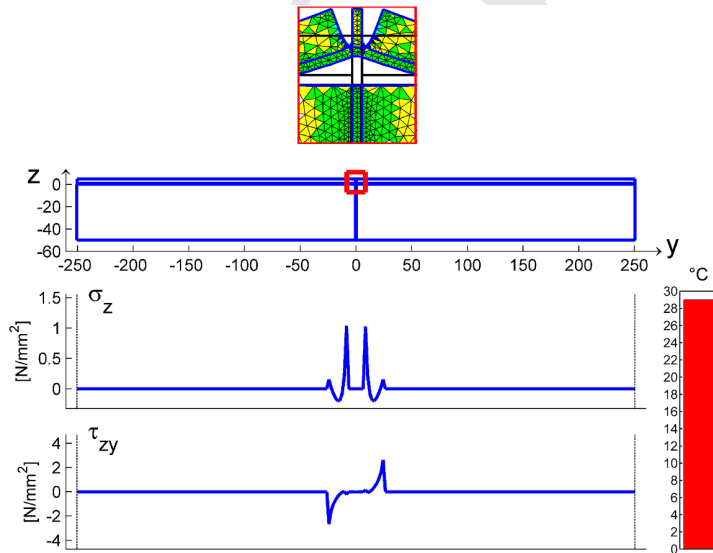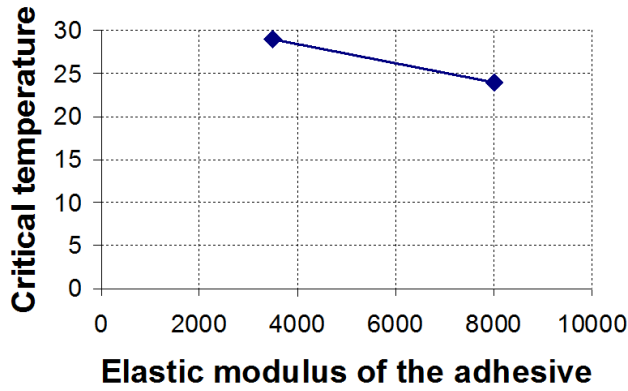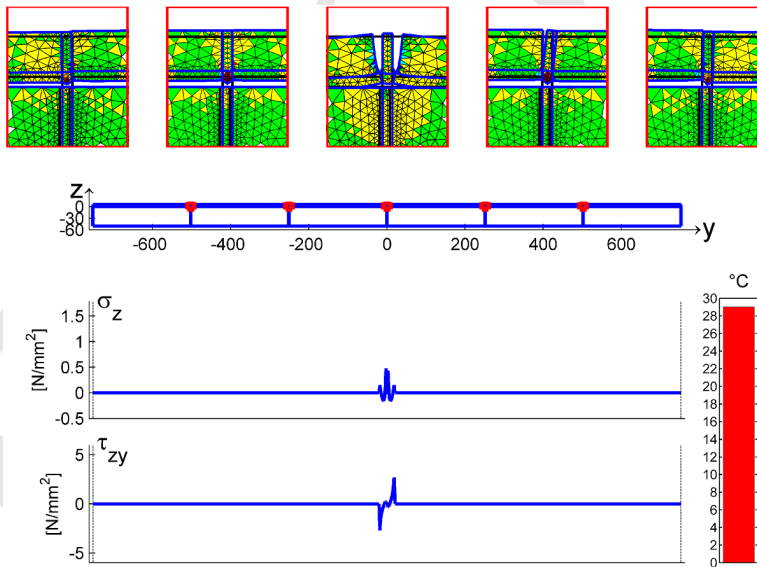

Figure 36: Stress analysis for the critical temperature in the model made of 6 tiles: final stage of crack propagation along the horizontal interface
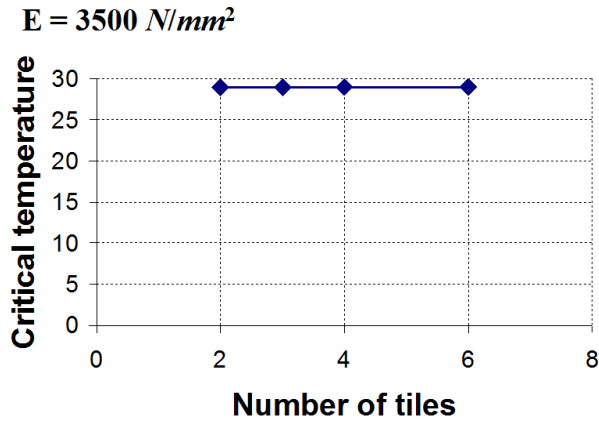
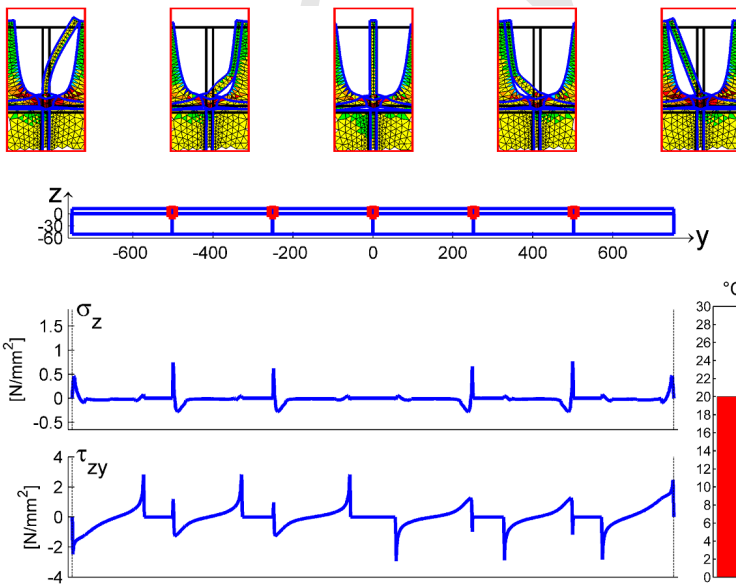Figure 37: Critical temperature in function of the number of tiles for $E = 3500 N/mm^2$

Figure 38: Stress analysis for tiles with a thickness of 12 *mm*: final stage of crack propagation for an increase in temperature of $20°C$
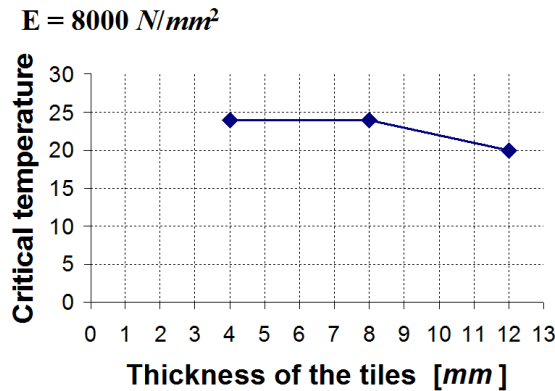
E = 8000 N/mm^2

Figure 39: Critical temperature in function of the height of the tiles

3.2   Parametric analysis on the height of the tiles

In Fig.38, we have increased the height of the tiles three-fold, obtaining tiles of traditional thickness (equal to 12 *mm*). The consequence is that the crack propagation on the horizontal interface does not start from the ends, as for the thin tiles, but from the corners of each tile. In particular, the cracks enucleate at the inner corners of the tiles and propagates outwards, toward the center of the tiles (the cracked portions of the horizontal interface in Fig.38 are those where both the normal and shear stresses are equal to 0). This happens for a $20°C$ variation in temperature, decreasing the critical temperature by $4°C$ compared to the model made with the same number of thin tiles (Fig.39).

In effect, we can identify two critical temperatures for this model, since the long propagation process activated for $20°C$ does not lead, in this model, to the complete separation of the tiles from the sub-base, which occurs at $23°C$. The final failure is reached when two cracks enucleate at the ends of the model and propagate inwards.

From this analysis, we can conclude that, using tiles of traditional thickness and keeping all the other geometrical and mechanical parameters constant, the horizontal interface under the grouting is more stressed and fails for a temperature lower than the failure temperature for thin tiles. Furthermore, the final critical temperature is lower than the failure temperature of the thin tiles.

3.3   Parametric analysis on the thickness of the grouting

In terms of the thickness of the grouting, the analyses performed for thicknesses of 1, 2, 3, 4 and 5 *mm* showed that this does not significantly affect the temper-
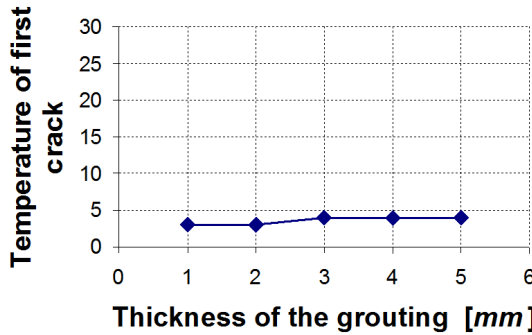
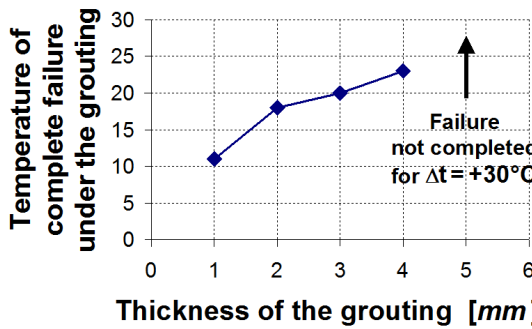Figure 40: Temperature of first crack in function of the thickness of the grouting

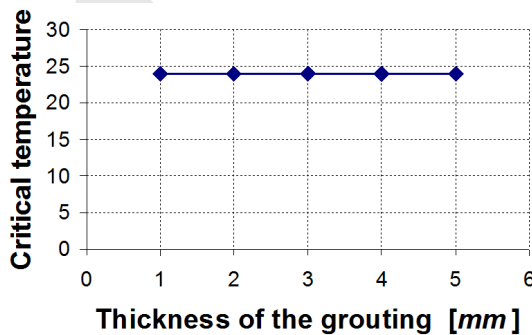Figure 41: Temperature of complete failure of the grouting in function of its thickness

Figure 42: Critical temperature in function of the thickness of the grouting

270 ature of first crack along the vertical interface (Fig. 40). The main effect is on
271 the temperature at which the grouting separates from the sub-base, a temperature
272 which increases with the thickness of the grouting (Fig.41). This occurs since the
273 greater thickness of the grouting reduces the stresses over the horizontal interface.
274 Nevertheless, the critical temperature is the same for all the cases: $24°C$ (Fig.42).

3.4 Parametric analysis on the thickness of the adhesive
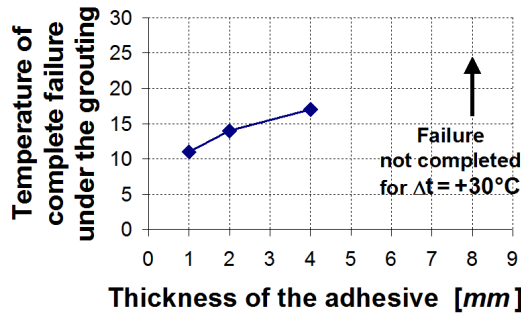
Figure 43: Temperature of complete failure of the grouting in function of the thickness of the adhesive
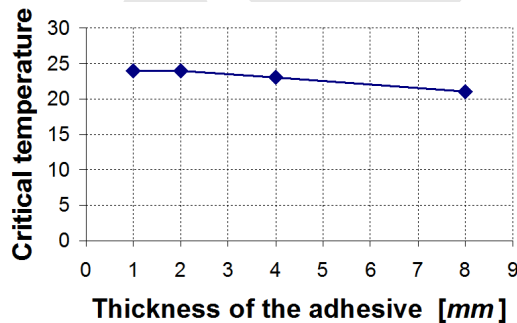
Figure 44: Critical temperature in function of the thickness of the adhesive

276 Our final analysis was performed on the thickness of the adhesive. We considered
277 thicknesses of 1, 2, 4 and 8 *mm*. In these cases, the parameter has opposite ef-
278 fects on the failure temperature of the grouting and the critical temperature. The
279 temperature at which the grouting separates from the sub-base increases with the
280 thickness of the adhesive (Fig.43), while the critical temperature progressively de-
281 creases when the thickness of the adhesive increases (Fig.44).

4   Conclusions

In this paper, it has been proven that the CM can be used to describe the damage effects deriving from the geometrical and elastic parameters of a radiant heat floor, finding that:

- The damaging process of thin tiles is different from the damaging effect of tiles of traditional thickness.

- Increasing the number of tiles does not change the critical temperature.

- Decreasing the Young modulus of the adhesive increases the critical temperature.

- Increasing the height of the tiles decreases the critical temperature.

- Increasing the height of the adhesive decreases the critical temperature.

- Increasing the thickness of the grouting does not change the critical temperature.

It follows that thin tiles work better than traditional tiles in radiant heat floors, in particular when the adhesive has a low elastic modulus and only a small thickness. We can therefore conclude that radiant heat floors are a very attractive possible field of development and design in the emerging market for thin tiles.

Acknowledgement

References

Blázquez, A.; París, F. (2011): Effect of numerical artificial corners appearing when using BEM on contact stresses. *Engineering Analysis with Boundary Elements*, vol. 35, no. 9, pp. 1029–1037.

Boe, C.; Rodriguez, J.; Plazaola, C.; Banfield, I.; Fong, A.; Caballero, R.; Vega, A. (2013): A Hydrodynamic Assessment of a Remotely Operated Underwater Vehicle Based on Computational Fluid Dynamic – Part 1 – Numerical Simulation. *CMES: Comput. Model. Eng. Sci.*, vol. 90, no. 2, pp. 165–177.

Chen C.Y.; Atkinson, C. (2009): The Stress Analysis of Thin Contact Layers: a Viscoelastic Case. *CMES: Comput. Model. Eng. Sci.*, vol. 48, no. 3, pp. 219–240.

313 **Chen, Y.; Cui, J.; Nie, Y.; Li, Y.** (2011): A New Algorithm for the Thermo-
314 Mechanical Coupled Frictional Contact Problem of Polycrystalline Aggregates Based
315 on Plastic Slip Theory. *CMES: Comput. Model. Eng. Sci.*, vol. 76, no. 3, pp.
316 189–206.

317 **Cocchetti, G.; Comi, C.; Perego, U.** (2011): Strength assessment of adhesively
318 bonded tile claddings. *International Journal of Solids and Structures*, vol. 48, no.
319 13, pp. 2048–2059.

320 **Dong, L.; Atluri, S.N.** (2012): SGBEM (Using Non-hyper-singular Traction BIE),
321 and Super Elements, for Non-Collinear Fatigue-growth Analyses of Cracks in Stiff-
322 ened Panels with Composite-Patch Repairs. *CMES: Comput. Model. Eng. Sci.*,
323 vol. 89, no. 5, pp. 415–456.

324 **Ferretti, E.** (2003a): Crack Propagation Modeling by Remeshing using the Cell
325 Method (CM). *CMES: Comput. Model. Eng. Sci.*, vol. 4, no. 1, pp. 51–72.

326 **Ferretti, E.** (2003b): Modeling of Compressive Tests on FRP Wrapped Concrete
327 Cylinders trough a Novel Triaxial Concrete Constitutive Law. *SITA: Scientific Is-
328 rael – Technological Advantages*, vol. 5, pp. 20–43.

329 **Ferretti, E.** (2004a): Crack-Path Analysis for Brittle and Non-Brittle Cracks: a
330 Cell Method Approach. *Computer Modeling in Engineering & Science (CMES)*,
331 vol. 6, no. 3, pp. 227-244.

332 **Ferretti, E.** (2004b): A Cell Method (CM) Code for Modeling the Pullout Test
333 Step-Wise. *CMES: Comput. Model. Eng. Sci.*, vol. 6, no. 5, pp. 453–476.

334 **Ferretti, E.** (2009): Cell Method Analysis of Crack Propagation in Tensioned Con-
335 crete Plates. *Computer Modeling in Engineering & Science (CMES)*, vol. 54, no.
336 3, pp. 253-282.

337 **Ferretti, E.** (2013): The Cell Method: an Enriched Description of Physics Starting
338 from the Algebraic Formulation. Submitted to *CMC: Comput. Mater. Con.*

339 **Ferretti, E.** (in press): *The Cell Method: a Purely Algebraic Computational Method
340 in Physics and Engineering Science*. Momentum Press.

341 **Ferretti, E.; Casadio, E.; Di Leo, A.** (2008): Masonry Walls under Shear Test: A
342 CM Modeling. *CMES: Comput. Model. Eng. Sci.*, vol. 30, no. 3, pp. 163–190.

343 **Han, Z.D.; Liu, H.T.; Rajendran, A.M; Atluri, S.N.** (2006): The Applications
344 of Meshless Local Petrov-Galerkin (MLPG) Approaches in High-Speed Impact,
345 Penetration and Perforation Problems. *CMES: Comput. Model. Eng. Sci.*, vol. 14,
346 no. 2, pp. 119–128.

347 **Hartmann, S.; Weyler, R.; Oliver, J.; Cante, J. C.; Hernández, J. A.** (2010): A
348 3D frictionless contact domain method for large deformation problems. *CMES:
349 Comput. Model. Eng. Sci.*, vol. 55, no. 3, pp. 211–269.

Imai, R.; Nakagawa, M. (2012): A reduction algorithm of contact problems for core seismic analysis of fast breeder reactors. *CMES: Comput. Model. Eng. Sci.*, vol. 84, no. 3, pp. 253–281.

Reaz Ahmed, S.; Deb Nath, S.K. (2009): A Simplified Analysis of the Tire-Tread Contact Problem using Displacement Potential Based Finite-Difference Technique. *CMES: Comput. Model. Eng. Sci.*, vol. 44, no. 1, pp. 35–64.

Schnack, E.; Weber, W.; Zhu, Y. (2011): Discussion of experimental data for 3D crack propagation on the basis of three dimensional singularities. *CMES: Comput. Model. Eng. Sci.*, vol. 74, no. 1, pp. 1–38.

Selvadurai, A.P.S; Atluri, S.N. (2010): *Contact Mechanics in Engineering Sciences*. Tech Science Press.

Theilig, H. (2010): Efficient fracture analysis of 2D crack problems by the MVCCI method. *Structural Durability and Health Monitoring*, vol. 6, no. 3-4, pp. 239–271.

Tonti, E. (2001): A Direct Discrete Formulation of Field Laws: the Cell Method. *CMES: Comput. Model. Eng. Sci.*, vol. 2, no. 2, pp. 237–258.

Willner, K. (2009): Constitutive Contact Laws in Structural Dynamics. *CMES: Comput. Model. Eng. Sci.*, vol. 48, no. 3, pp. 303–336.

Yun, C.; Junzhi, C.; Yufeng, N.; Yiqiang, L. (2011): A New Algorithm for the Thermo-Mechanical Coupled Frictional Contact Problem of Polycrystalline Aggregates Based on Plastic Slip Theory. *CMES: Comput. Model. Eng. Sci.*, vol. 76, no. 3, pp. 189–206.

Zhang, Y.; Noda, N.-A.; Takaishi, K. (2011): Effects of geometry on intensity of singular stress fields at the corner of single-lap joints. *World Academy of Science, Engineering and Technology*, vol. 79, pp. 911–916.

Zheng, G.; Li, Z.-W. (2012): Finite element analysis of adjacent building response to corner effect of excavation. *Tianjin Daxue Xuebao (Ziran Kexue yu Gongcheng Jishu Ban)/Journal of Tianjin University Science and Technology*, vol. 45, no. 8, pp. 688–699.

Zhou, Y.-T.; Li, X.; Yu, D.-H.; Lee, K.-Y. (2010): Coupled crack/contact analysis for composite material containing periodic cracks under periodic rigid punches action. *CMES: Comput. Model. Eng. Sci.*, vol. 63, no. 2, pp. 163–189.